



HAL
open science

Towards the prediction of hydrothermal ageing of 3Y-TZP bioceramics from processing parameters

Chong Wei, Laurent Gremillard

► **To cite this version:**

Chong Wei, Laurent Gremillard. Towards the prediction of hydrothermal ageing of 3Y-TZP bioceramics from processing parameters. *Acta Materialia*, 2018, 144, pp.245 - 256. 10.1016/j.actamat.2017.10.061 . hal-01758663

HAL Id: hal-01758663

<https://hal.science/hal-01758663>

Submitted on 5 Mar 2019

HAL is a multi-disciplinary open access archive for the deposit and dissemination of scientific research documents, whether they are published or not. The documents may come from teaching and research institutions in France or abroad, or from public or private research centers.

L'archive ouverte pluridisciplinaire **HAL**, est destinée au dépôt et à la diffusion de documents scientifiques de niveau recherche, publiés ou non, émanant des établissements d'enseignement et de recherche français ou étrangers, des laboratoires publics ou privés.

Towards the prediction of hydrothermal ageing of 3Y-TZP bioceramics from processing parameters.

Published in Acta Materialia (2018) vol. 144, pp. 245-56,
<https://doi.org/10.1016/j.actamat.2017.10.061>

Chong Wei, Laurent Gremillard

Univ. Lyon, INSA-Lyon, MATEIS, UMR CNRS 5510, 7 Avenue Jean Capelle, 69621
Villeurbanne, France

Abstract

Hydrothermal ageing of yttria-stabilized tetragonal zirconia ceramics can have a strong influence on the lifetime of zirconia devices. Ageing kinetics are often described by the Mehl–Avrami–Johnson equation, most often used as a phenomenological description. This work seeks to relate the parameters of MAJ equations (V_{\max} , n , b_0 and Q) to microstructural characteristics of the zirconia material: grain sizes, Y_2O_3 partitioning, monoclinic, tetragonal and cubic phases ratio. Samples with identical nominal composition of 3Y-TZP were prepared with grain sizes ranging from 190 nm to 773 nm. From their microstructural parameters, a relationship between microstructural parameters and sintering cycles was first proposed, followed by a relationship between ageing parameters and microstructural parameters. These results provide a convenient framework to better develop the sintering cycle of zirconia biomaterial in order to maximize their resistance to hydrothermal ageing.

1. Introduction

Zirconia-based materials, especially yttria-stabilized tetragonal zirconia polycrystals (Y-TZP), exhibit the best mechanical properties of oxide ceramics: this is the consequence of phase transformation toughening, which increases its crack propagation resistance [1-3]. Furthermore, they are high-temperature resistant and offer low thermal conductivity, good ionic conductivity, good biocompatibility and superior aesthetic appearance [2]. Therefore Y-TZP ceramics are very attractive for a wide range of biomaterial applications such as fixed-partial denture in restorative dentistry or femoral heads in orthopedics [4,5]. Large efforts were already devoted to the study of mechanical properties of zirconia-based ceramics, but also of their sensitivity to low temperature degradation (LTD). Low-Temperature Degradation of zirconia (also called hydrothermal ageing) can be summarized as follows: the presence of water in the environment of zirconia pieces triggers the tetragonal to monoclinic (t-m) transformation of some grains on the surface, which potentially leads to roughening and micro-cracking because of the high volume increase (~5%) associated to the t-m transformation. Hydrothermal ageing is driven by the annihilation of oxygen vacancies by water-derived species [6,7]. This process both destabilize the tetragonal phase and

overstabilizes the monoclinic one [8]. Ageing kinetics are usually described by the Mehl–Avrami–Johnson equation [9] (eq. 1).

$$\frac{V_m - V_0}{V_{\max} - V_0} = 1 - \exp(-(b \cdot t)^n) \quad (1)$$

In this equation, the parameter b is thermally activated: $b = b_0 \exp\left(\frac{-Q}{RT}\right)$.

V_m is the monoclinic phase content after ageing during a duration t at absolute temperature T , V_0 and V_{\max} are the initial and saturation levels of monoclinic phase content, and R is the ideal gas constant. Q is the activation energy, typically around 100 kJ/mol. The value of the parameter n is typically between 0.3 and 3.5 [10].

Many factors such as different grain size, residual or applied stresses, density, content of Y_2O_3 in tetragonal phase, proportion of cubic phase, doping with more than one oxide, can influence the ageing process [4, 11-17]. A few examples of these influences are given below. Jansen *et al.* reported that doping with ceria or decreasing the grain size strongly improved the ageing resistance of Y-TZP [18]. For instance, 3Y-TZP ceramics with grain size lower than 100 nm exhibit almost no ageing, whereas submicrometric 3Y-TZP ceramics may undergo severe degradation under the same conditions [19]. A critical value of grain size around 300 nm, below which ageing processes do not occur, was sometimes proposed [14], but later researches showed that this critical value has no physical basis [20] and may be dependent on other materials parameters [21]. Chevalier *et al.* reported that cubic grains are enriched by yttrium, which in turn leads to a decrease of the yttrium content in the neighboring tetragonal grains, making these Y-poor tetragonal grains more susceptible to transformation into monoclinic phase and thus affecting the ageing behavior of zirconia [12].

However, all the parameters mentioned above are interdependent, in particular through processing parameters: for instance, increasing the sintering time may increase both the grain size and the proportion of cubic phase [22], and the amount of cubic phase may also influence internal stresses. It is thus quite difficult to understand what parameters directly influence ageing [23]. Therefore, by carefully analyzing the microstructure and ageing behavior of several zirconia ceramics fabricated from the same powder, this paper seeks to isolate and quantify the influence of grain sizes, content of Y_2O_3 in tetragonal phase and amount of cubic phase on ageing kinetics parameters (V_{\max} , n , b_0 , Q) of 3Y-TZP.

2. Materials and methods

2.1. Material preparation

The samples were fabricated starting from Y-TZP powders (TZ3YE, Tosoh, Japan). TZ3YE contains 3mol% (5.2wt%) yttria plus controlled alumina and silica doping. The zirconia green bodies used in the present study were prepared by slip casting. Firstly, the slurry were prepared by dispersing 150 g of TZ3YE powder in 37.5 g H_2O , using 2.25 g Darvan 821A as dispersant. Complete dispersion was achieved by ball milling with 150 g Y-TZP milling balls during 48 hours. The resulting slurries were then cast in porous plaster molds and dried in air at 25°C for 7 days. Finally the green bodies were sintered in a programmable electrical furnace, under different sintering conditions so as to obtain different microstructures: two materials were obtained by conventional sintering (samples 1430-2h and 1430-5h); two other materials were obtained by two step sintering (conditions chosen to obtain fully dense materials with small grain size [24]: TSS1 and TSS2 materials); finally some series of samples obtained using the TSS2 sintering conditions were submitted to different post-

sintering thermal treatment in order to modify their microstructure (materials PS1150-100h, PS1150-200h, PS1430-20h, PS1500-2h, PS1550-20h). The exact sintering cycles used for all materials are summarized in table 1. All samples (at least 6 per material) were shaped as 10x10 mm plates, polished, and annealed after polishing to remove any extra residual stress possibly induced by machining and polishing. The density of all samples was then measured by using Arthur's method, based on Archimede's principle.

Table 1: List of samples: processing hydrothermal ageing conditions; TSS stands for "Two Steps Sintering", PS for "Post Sintering" (post sintering heat treatment applied to TSS2 materials).

Sample	sintering condition	annealing conditions	aging temperature/°C	density
TSS1	T1 1300°C T2 1150°C-15h	1150°C-1h	85, 110, 134, 140	6.04
TSS2	T1 1280°C T2 1150°C-25h	1150°C-1h	85, 110, 134, 140	6.07
1430-2h	1430°C-2h	1250°C-0.5h	85, 110, 134, 140	6.05
1430-5h	1430°C-5h	1250°C-0.5h	85, 110, 134, 140	6.04
PS1150-100h	TSS2+post sintering 1150°C-100h		134 + stepwise procedure	6.07
PS1150-200h	TSS2+post sintering 1150°C-200h		134 + stepwise procedure	6.07
PS1430-20h	TSS2+post sintering 1430°C-20h		134 + stepwise procedure	6.07
PS1500-2h	TSS2+post sintering 1500°C-2h		134 + stepwise procedure	6.07
PS1550-20h	TSS2+post sintering 1550°C-2h		134 + stepwise procedure	6.07

2.2. Microstructural analyses: grain size, proportion of cubic phase, yttria content

SEM observations were conducted using a Zeiss Supra55 VP microscope. For each group of samples, grain size was obtained from micrographs taken on both side of 4 samples, using the linear intercept method, and multiplying by 1.56 the average linear intercept length of at least 500 grains to correct the fact that they were intercepted at random positions (not necessarily at their diameter) in accordance with the method developed by Mendelsohn et al. [25].

The average Y_2O_3 content in tetragonal phase and amount of cubic phase were obtained from XRD data (using a D8 Advance diffractometer, Bruker, Germany, with step size 0.02 deg and scan speed 1 s/step). To summarize, first a calibration curve of the amount of Y_2O_3 in the cubic and tetragonal phases *versus* the lattice parameters was established, from PDF files and previous work by other authors [26-28] (Fig.1). Then XRD patterns were recorded (on one sample per group) over a large angular range (15-120 deg. 2θ) and analyzed using an iterative procedure based on Rietveld refinement. Rietveld refinement was conducted with Topas 4.0 software (Bruker), using a fundamental parameters approach; only scale factors, lattice parameters, crystallite size and systematic diffractometer-related angular errors were set free during the refinements. The outcomes of the first iteration of Rietveld refinement were mainly the approximate proportions of the different phases (cubic and tetragonal) and the lattice parameters of the tetragonal phase (in most materials cubic peaks were lost in the background or convoluted with some tetragonal peaks). The amount of yttria in the tetragonal phase was then calculated from the calibration curve. Since the total amount of Y_2O_3 is known (3 mol.%) from the composition of the powder, it was thus possible to determine the amount of yttria in the cubic phase (considering the approximate proportion of cubic phase) and thus its lattice parameter. The next iterations were conducted while setting the cubic

phase lattice parameter as a constant (calculated from the amount of yttria in the cubic phase), which allowed evaluating more and more precise phases proportions and tetragonal phase lattice parameter, thus recalculating a more and more precise cubic phase lattice parameter. The iterations were continued until convergence (2 to 4 iterations generally allowed convergence to the 3rd digit for the proportion of the phases and to the 6th digit for the lattice parameters).

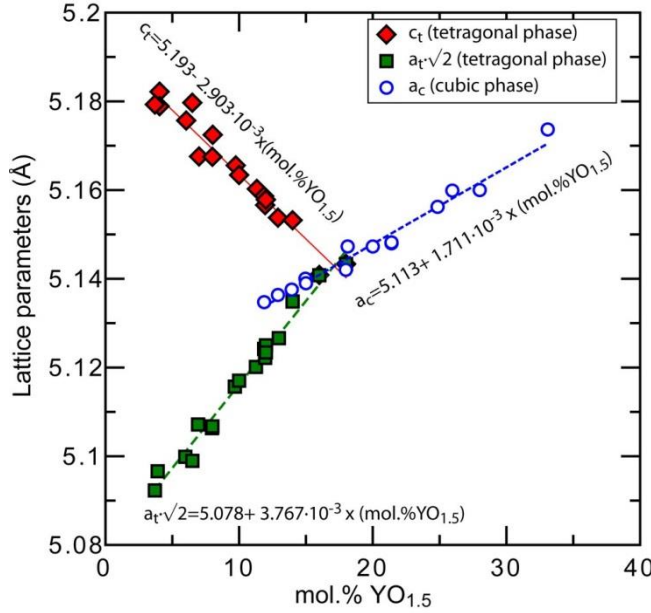


Figure 1: Calibration curve giving the lattice parameters of tetragonal and cubic zirconia vs yttrium amount.

2.3. Assessment of ageing kinetics parameters.

Ageing kinetics were evaluated by performing accelerated ageing tests on all samples in water vapour in an autoclave (Wolf Sanoclav), at temperatures ranging from 80 to 150°C.

The amount of tetragonal to monoclinic phase transformation was measured at different time points by X-ray diffraction (XRD). XRD patterns were recorded in the 27-33° (2θ) range with a scan speed of 0.2 deg·min⁻¹ and a step size of 0.05°, using a Bruker D8-advance diffractometer. The monoclinic ZrO₂ phase content (V_m) [29] was calculated as:

$$V_m = \frac{1.311X_m}{1 + 0.311X_m} \quad (2 - a)$$

In which the value of X_m was determined directly from the diffraction diagrams using Garvie and Nicholson's equation [30]:

$$X_m = \frac{I_m^{-111} + I_m^{111}}{I_m^{-111} + I_m^{111} + I_t^{101}} \quad (2 - b)$$

Where I_p^{hkl} is the area of the diffraction peak related to the (hkl) plane of phase p (m for monoclinic and t for tetragonal).

The hydrothermal ageing kinetics were rationalized by fitting the transformation curves with the Mehl–Avrami–Johnson laws [9] as explained in the introduction. For materials TSS1,

TSS2, 1430-2h and 1430-5h, complete ageing kinetics were recorded at 140, 134, 110 and 85°C (one sample per temperature); then the ageing parameters (V_0 , V_m , b_0 , Q , n) were obtained using a fitting procedure consisting in minimizing the total quadratic error between the calculated kinetics and the experimental points.

In addition, stepwise ageing procedures [31] were designed as indicated in Table 2 in order to determine the values of Q , and b_0 for sample PS1150-200h, PS1430-20h, PS 1500-2h, PS1550-2h (for all these materials, a complete kinetics at 134°C was also performed). The stepwise procedure is based on ageing measurements at different temperature on a single sample, and can largely reduce the time necessary for correct extrapolations. Following this procedure, PS1430-20h, PS 1500-2h and PS1550-2h materials (2 samples each) were aged between 80°C and 134°C; due to much slower ageing kinetics, PS1150-200h material (2 samples) was aged using a specific stepwise procedure, between 80°C and 150°C.

Table 2: Stepwise ageing procedure for PS1150-200h, PS1430-20h, PS 1500-2h, PS1550-2h; the procedure for PS1150-200h involves much longer ageing duration because ageing of PS1150-200h is much slower than for other materials.

PS1150-200h		PS1430-20h, PS 1500-2h, PS1550-2h	
T_i (°C)	Δt_i (h)	T_i (°C)	Δt_i (h)
150	26	134	2
141	20	141	2
110	100	110	30
121	50	121	18
134	25	100	75
100	145	90	178
90	267	80	265
80	259		

For the stepwise ageing procedure, equation (3) is used for initial assessment of the Q value, before an optimization procedure takes place to determine V_0 , V_m , b_0 , Q and n (for detailed process, see reference [31]):

$$\ln \left[\frac{1}{\Delta t_i} \ln \left(\frac{V_{max} - V_{i-1}}{V_{max} - V_i} \right) \right] \approx \ln(n b_0) - \frac{Q}{RT_i} \quad (3)$$

3. Results

3.1 Microstructural analyses

Density higher than 99% of the theoretical density (6.08) was achieved for all samples (density values are summarized in table 1). Fig.2 shows SEM micrographs of all the specimens. Even though they were manufactured using the same powder, due the different sintering thermal treatments the samples exhibit grain sizes ranging from 190 to 779 nm. Very fine-grained zirconia ceramics were obtained by two step sintering, while materials with larger grains were obtained by conventional sintering.

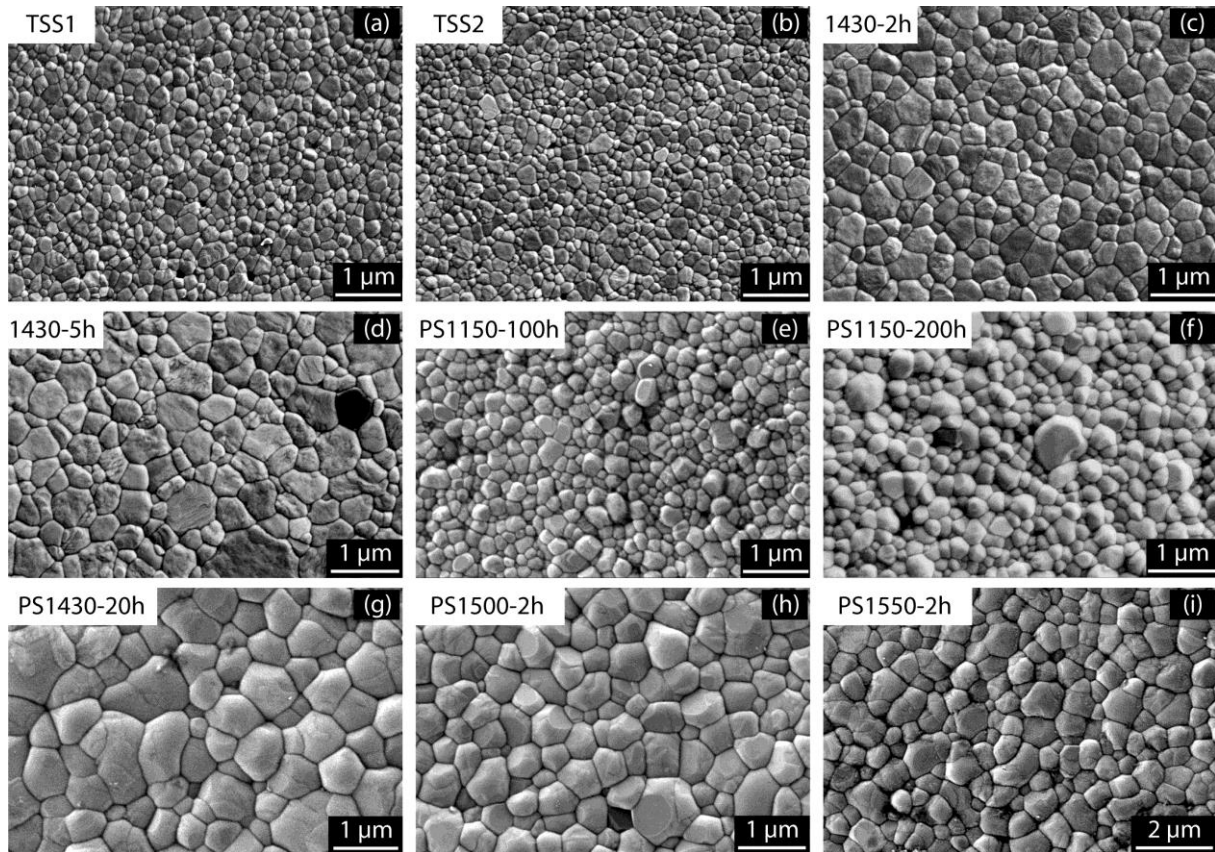


Figure 2: SEM micrographs of all specimens after annealing

The phase content and phase partitioning were analyzed by X-ray diffraction coupled to Rietveld analysis. The results of these microstructural analyses are shown in table 3. Figure 3 illustrates the quantification of cubic phase by Rietveld analysis, on two extreme cases: the cubic peaks are hardly visible in TSS1 (that contain 10 wt.% of cubic phase), while it's detectable “with the naked eye” on 1430-2h (18% of cubic phase).

Table 3: Microstructural features of zirconia materials before aging

Sample	wt.% cubic	mol% Y_2O_3 in tetragonal	Grain size (nm)	mol% Y_2O_3 in cubic
TSS1	0.107	2.90	210	3.84
TSS2	0.117	2.87	190	3.97
PS1150-100h	0.151	2.58	290	5.33
PS1150-200h	0.175	2.34	320	6.16
PS1430-20h	0.304	2.13	750	4.75
1430-2h	0.176	2.55	410	4.81
1430-5h	0.205	2.41	520	5.30
PS1500-2h	0.263	2.37	600	4.75
PS1550-2h	0.268	2.34	770	4.80

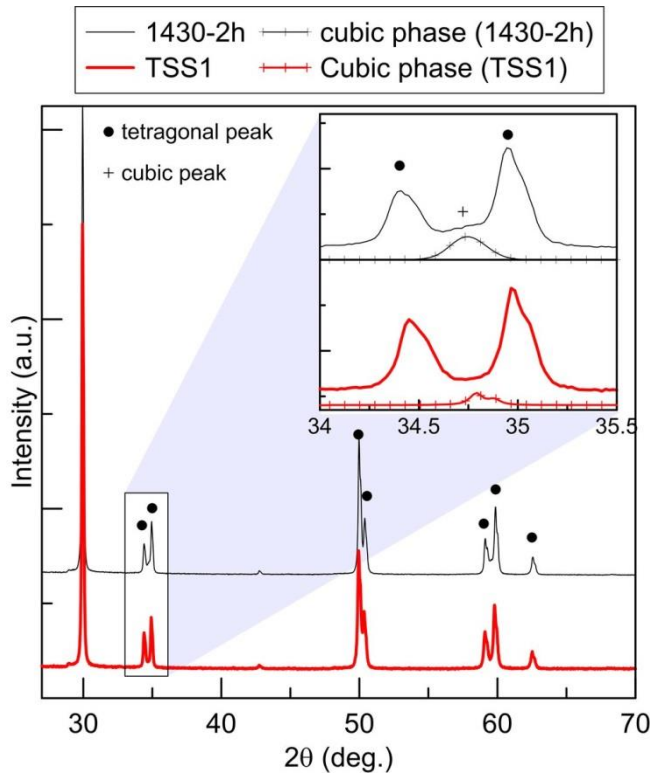


Figure 3: X-ray diffractograms of TSS1 (red, bold line) and 1430-2h (black, thin line); the inset shows a detail of the diagram around 35 deg. 2θ : tetragonal doublet around a cubic peak.

A few trends can be distinguished from these data. In particular, for a given sintering temperature (here, 1430°C or 1150°C), the content of Y_2O_3 in tetragonal phase decreases linearly and the content of cubic phase increase linearly with increasing holding time (Fig.4); the variation are faster with increasing sintering temperature. Moreover, the grain size increases with increasing holding time.

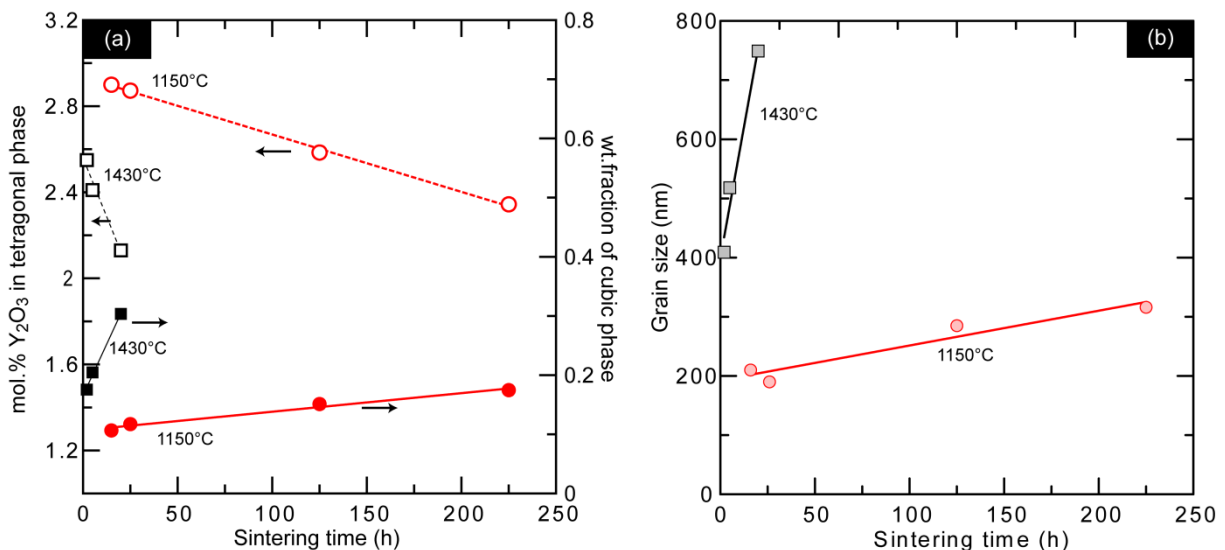


Figure 4: (a) Y_2O_3 content in tetragonal phase (open symbols), proportion of cubic phase (full symbols) and (b) grain size (light symbols) versus holding time for sintering cycles at 1430°C (squares) or 1150°C (discs).

For identical holding times during sintering (here, 2 hours), the Y_2O_3 content in tetragonal phase decreases and the content of cubic phase increases with increasing sintering temperature (Fig. 5). In the same conditions, the grain size increases linearly with increasing sintering temperature (Fig. 5). Thus both higher sintering temperatures and longer dwell times can increase the grain size. Figure 4 shows that the grain size is much more sensitive to sintering temperature than to sintering time.

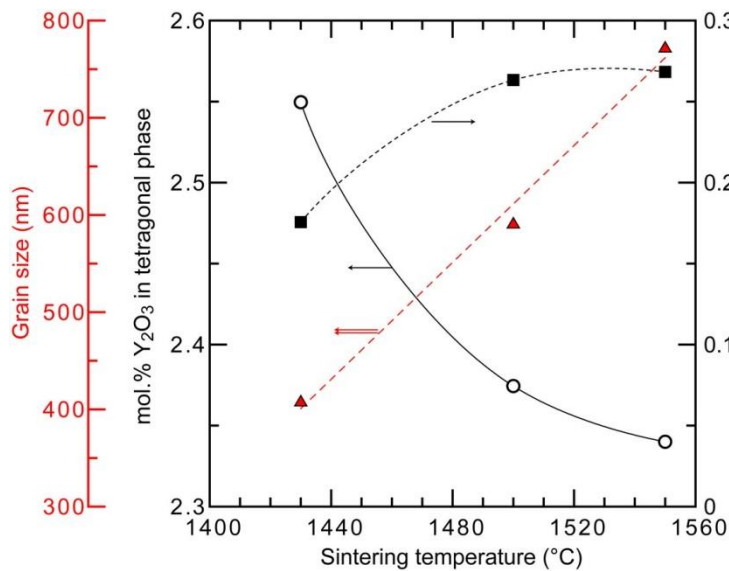


Figure 5: Y_2O_3 content in tetragonal phase (open circles), proportion of cubic phase (squares) and grain size (triangles) versus sintering temperature for a 2h holding time during sintering.

Fig.6 illustrates the interdependence between grain size, proportion of cubic phase and Yttria content in the tetragonal phase. It shows that the grain size increases linearly with the proportion of cubic phase, while the Y_2O_3 content in tetragonal phase decreases linearly with increasing proportion of cubic phase. As a result, the Y_2O_3 content in tetragonal phase decreases when the grain size increases.

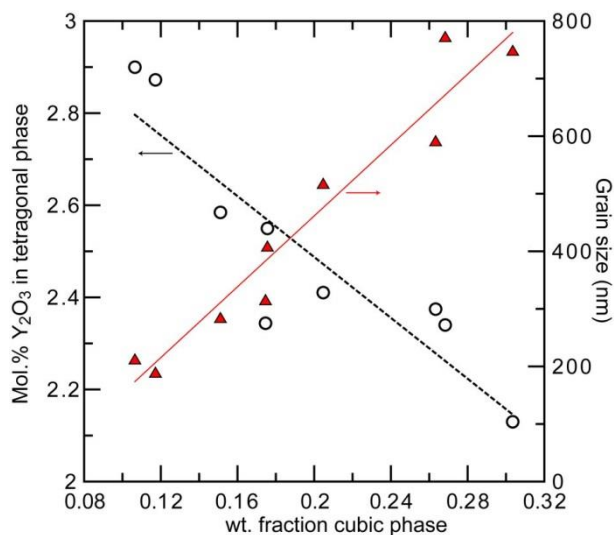


Figure 6: Y_2O_3 content in tetragonal phase (open circles) and grain size (triangles) versus the content of cubic phase.

3.2 Ageing kinetics

TSS1 and TSS2 samples do not suffer from ageing, even after more than 2700 hours autoclave at 134°C, 1500 hours at 140°C and 3000 hours at 90°C.

The surface phase transformation curves for the other samples as a function of the hydrothermal ageing time are shown in Fig.7. The ageing kinetics measured at 134 °C are shown in Fig.8. PS1430-20h, PS1500-2h, PS1550-2h, 1430-2h and 1430-5h materials exhibit a similar ageing behavior, while PS1150-200h and PS1150-100h age much more slowly. These results are apparently coherent with the existence of a grain-size threshold (~300 nm [14]) under which hydrothermal ageing is not measurable using XRD.

The parameters of MAJ equation of the different samples were obtained using the procedure described in section 2.3, and reported in table 4. Unfortunately, these parameters could not be evaluated on PS1150-100h (this material ages too slowly: less than 10% monoclinic phase after 3000h ageing). For all materials considered here, the value of Vmax increases approximately linearly with increasing grain size and content of cubic phase and decreasing content of Y₂O₃ in tetragonal phase. The value of n decreases slightly with increasing grain size and content of cubic phase. When considering the values of b₀ and Q, two groups of samples can be distinguished: most materials show b₀ around 10¹³ and Q around 115 kJ/mol, while PS1150-200h stands out with much lower values for both parameters (b₀=8·10² and Q=41 kJ/mol). As a result, PS1150-200h ages very slowly at 134°C, but faster than all other samples at 37°C (fig. 8); this is obvious from the values of b at 134 and 37°C in table 4. The knowledge of Q also allows to establish the time-temperature equivalence: 1h in an autoclave at 134 °C represents around 5 years of hydrothermal ageing *in vivo* at 37°C for 1430-2h, 1430-5h, PS1430-20h, PS1500-2h and PS1550-2h samples, but 44h at 37°C for PS1150-200h samples. From Table 4 it can be determined that the 1430-5h sample has the best ageing resistance (lowest value of b) at 37°C.

Table 4: Parameters of MAJ equation of the different materials

samples	Vmax	n	b (134°C) (h ⁻¹)	b (37°C) (h ⁻¹)	b ₀	Q (kJ/mol)
1430-2h	0.82	1.00	5.66·10 ⁻²	1.19·10 ⁻⁶	5.01·10 ¹³	116.4
1430-5h	0.8	0.88	4.61·10 ⁻²	1.07·10 ⁻⁶	2.98·10 ¹³	115.3
PS1150-200h	0.85	0.99	4.38·10 ⁻³	1.00·10 ⁻⁴	7.67·10 ²	40.8
PS1430-20h	0.77	0.83	6.94·10 ⁻²	1.42·10 ⁻⁶	6.73·10 ¹³	116.7
PS1500-2h	0.79	0.92	5.04·10 ⁻²	1.13·10 ⁻⁶	3.65·10 ¹³	115.7
PS1550-2h	0.78	0.89	7.32·10 ⁻²	2.18·10 ⁻⁶	2.13·10 ¹³	112.6

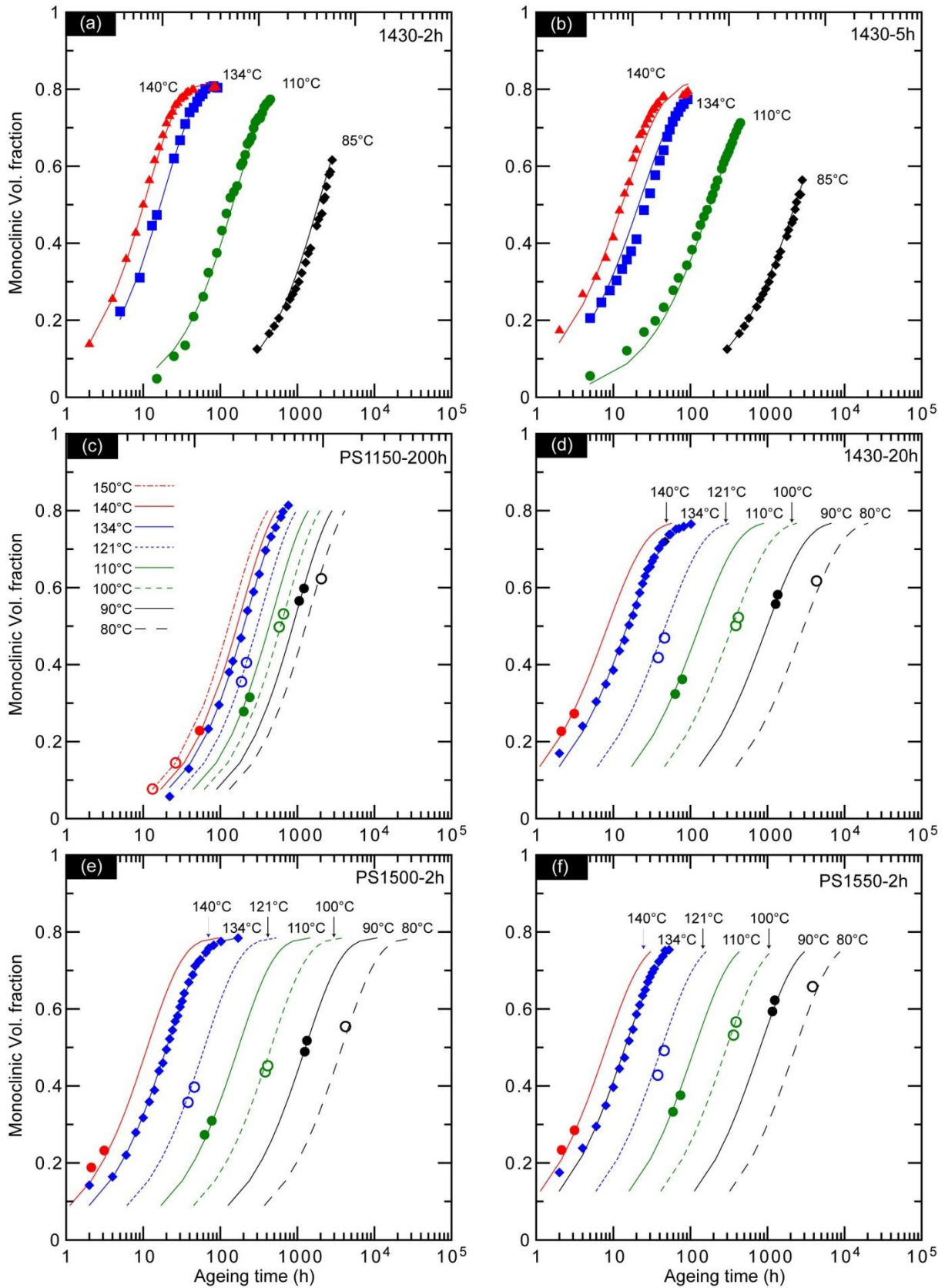


Figure 7: Hydrothermal ageing kinetics between 80 and 140°C for samples 1430-2h (a), 1430-5h (b), PS1150-200h(c), PS1430-20h (d), PS1500-2h (e), PS1550-2h (f).

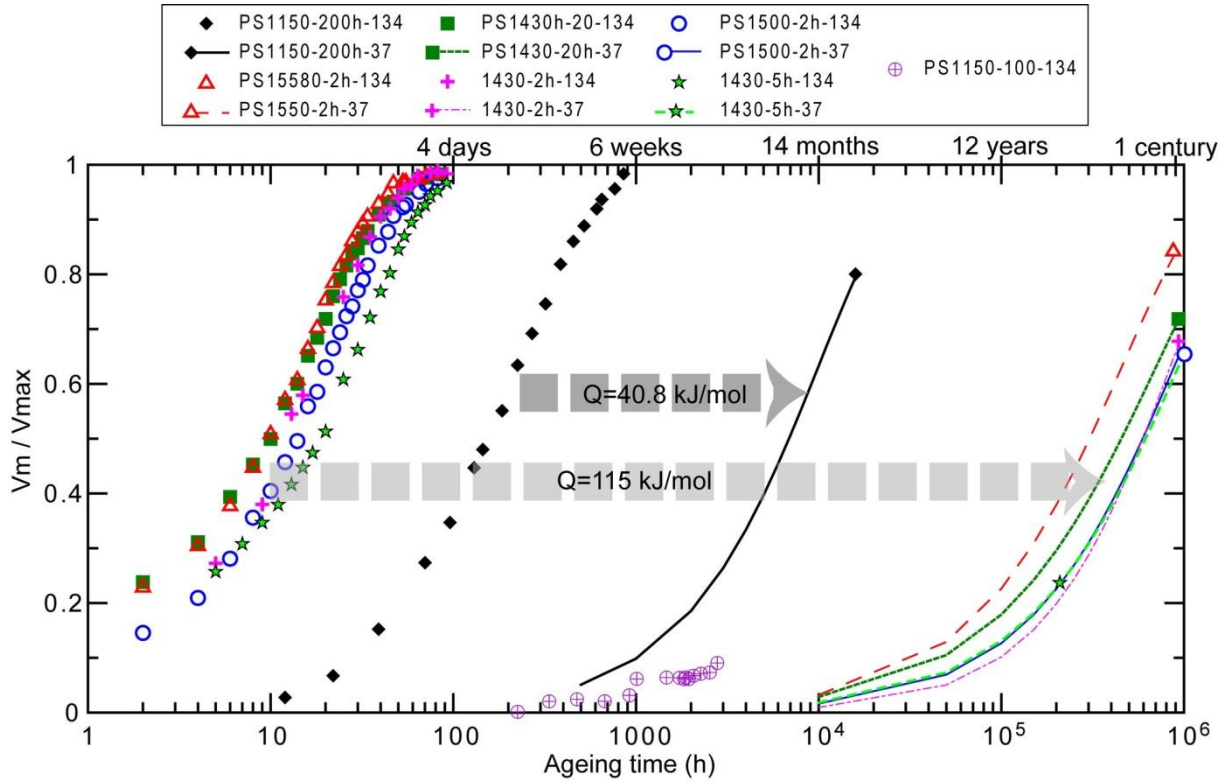


Figure 8: Ageing kinetics of all samples at 134 °C (symbols) and 37°C (dotted lines).

4. Discussion

4.1 Correlation analysis of structural parameters and sintering cycle

In order to be able to better develop the sintering cycle, the results of this work can be combined to determine a relationship between structural parameters and sintering cycle. A few hypotheses can guide the choice of simple mathematical, phenomenological models for these relationships.

At constant temperature, the formation of cubic phase from tetragonal grains follows a nucleation and growth mechanism (nucleation being driven by Y diffusion [32]), thus can be described by a MAJ law (Eq. 4).

$$f(T, t) = f_0 + (f_{max} - f_0)(1 - \exp(-(c \cdot t)^{n_c})) \quad (4)$$

In this equation, the parameter c is thermally activated: $c = c_0 \exp\left(\frac{-Q_c}{RT}\right)$; f is the cubic phase content obtained after the sintering process during a duration t at absolute temperature T , f_0 and f_{max} are the initial and saturation levels of cubic phase content, and R is the gas constant. Q_c is an apparent activation energy for the formation of cubic phase. Theoretically, f_{max} could be calculated from the yttria-zirconia phase diagram (f_{max} is determined by the temperature and the content of yttria). However, on the one hand this work involves rather complicated thermal treatments (two-step sintering and post-sintering annealing), and on the other hand after most thermal treatments the equilibrium phase partitioning may not be reached (thus the equilibrium phase diagram is not useful); thus it is easier and more correct to consider f_{max} as an adjustable parameter.

Assuming a homogeneous initial distribution of Yttrium, the Yttrium concentration in the tetragonal phase is directly controlled by the diffusion of Y from the tetragonal phase to the

grain boundaries and to the cubic phase [32]. Thus again a decreasing exponential law can be applied (eq. 5).

$$y(T, t) = y_0 - y_{dmax} \cdot (1 - \exp(-(s \cdot t)^{n_y})) \quad (5)$$

In this equation, the parameter s is thermally activated: $s = s_0 \exp\left(\frac{-Q_s}{RT}\right)$; y is the content of Y_2O_3 in tetragonal phase during sintering process during a duration t at absolute temperature T , y_0 is the initial content of Y_2O_3 in tetragonal phase, y_{dmax} are the maximum content of Y_2O_3 diffusing into the cubic phase, and R is the gas constant. Q_s is the apparent activation energy for yttrium diffusion.

Finally, since TZ3YE powder contains small amounts of alumina and silica that are mainly located at the grain boundaries as solute species, an equation of grain growth taking solute drag into account [33] can be used (Eq. 6).

$$D^3(T, t) = D_0^3 + d \cdot t \quad (6)$$

In this equation, the parameter d is thermally activated: $d = d_0 \exp\left(\frac{-Q_d}{RT}\right)$; D is the grain size during sintering process during a duration t at absolute temperature T , D_0 is the initial grain size, and R is the gas constant. Q_d is the apparent activation energy for grain growth.

Then a numerical solver (“GRG Nonlinear solver” implemented in Microsoft Excel, based on the Generalized Reduced Gradients method) is used to determine these parameters (f_{max} , f_0 , n_c , c_0 , Q_c , y_0 , y_{dmax} , n_y , s_0 , Q_s , D_0 , d_0 , Q_d), taking into account all steps of the sintering treatment; their optimized values are shown in table 5. These calculations result in a good agreement between the calculated values of grain size, proportion of cubic phase and yttrium concentration in the tetragonal phase (obtained from the parameters in table 3) and their experimental values, as shown in Figure 9.

Table 5: Summary of the parameter of the microstructural models (equations (4) to (6)).

Cubic content	f_{max}	n_c	Q_c (kJ/mol)	c_0	f_0
	0.45	0.48	350.5	$2.46 \cdot 10^9$	0.078
Mol. % Y_2O_3 (in t)	y_{dmax}	n_y	Q_s (kJ/mol)	s_0	y_0
	1	0.68	278.1	$9.86 \cdot 10^7$	3.1
Grain size (nm)	D_0 (nm)	d_0 (m ² /s)	Q_d (kJ/mol)		
	221.2	$2.0 \cdot 10^{42}$	895.6		

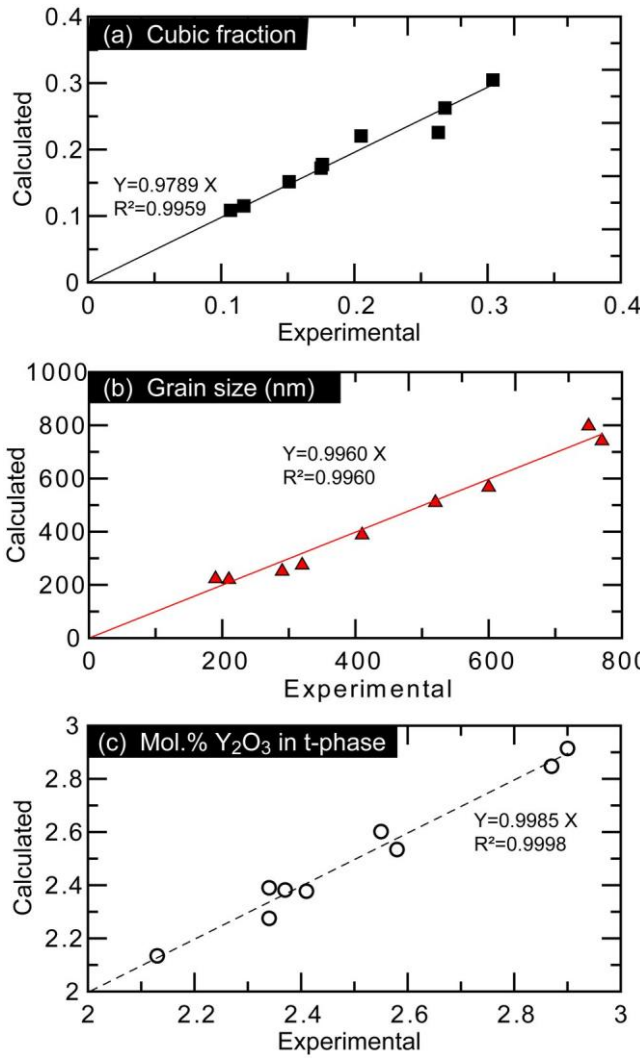


Figure 9: Comparison of the calculated and experimental values of f , y , D . Both the slopes of the trend lines and the R^2 values, close to 1, show a good agreement between measured and calculate values.

4.2 Prediction of ageing kinetics parameters from micro structural parameters

Activation energies for ageing (Q) between 41 and 117 kJ/mol were found (table 4). Due to scattering of the measured monoclinic fraction data, it was decided that differences of less than 2 kJ/mol were not significant, thus the average activation energy (115.3 ± 1.6 kJ/mol) of samples 1430-2h, 1430-5h, PS1430-20h, PS1500-2h and PS1550-2h was attributed to all these samples. The same argument applies for n , thus the average value of n (0.92) was chosen for all samples. Finally the parameters V_{max} and b_0 were recalculated according to these new values of n and Q (Table 6).

Then a multiple regression analysis (equations (7) and (8)) was applied to calculate the evolutions of $\frac{b_0 - \langle b_0 \rangle}{\sigma_{b_0}}$ and $\frac{V_{max} - \langle V_{max} \rangle}{\sigma_{V_{max}}}$ versus $(\frac{f - \langle f \rangle}{\sigma_f}, \frac{y - \langle y \rangle}{\sigma_y}$ and $\frac{D - \langle D \rangle}{\sigma_D})$ (here, $\langle x \rangle$ is the average value of x and σ_x is its standard deviation).

$$\frac{b_0 - \langle b_0 \rangle}{\sigma_{b_0}} = a_f^b \cdot \frac{f - \langle f \rangle}{\sigma_f} + a_y^b \cdot \frac{y - \langle y \rangle}{\sigma_y} + a_D^b \cdot \frac{D - \langle D \rangle}{\sigma_D} \quad (7)$$

$$\frac{V_{max} - \langle V_{max} \rangle}{\sigma_{V_{max}}} = a_f^V \cdot \frac{f - \langle f \rangle}{\sigma_f} + a_y^V \cdot \frac{y - \langle y \rangle}{\sigma_y} + a_D^V \cdot \frac{D - \langle D \rangle}{\sigma_D} \quad (8)$$

This approach was attempted using measured values of f , y and D summarized in table 6. The values of a_f , a_y , a_D obtained are summarized in Table 7, and the absolute value of these

coefficients can reflect the degree of correlation of the corresponding parameters. The calculated evolutions of V_{max} and b_0 are summarized in Fig.10.

In such a linear regression (that uses only standardized data) the highest coefficients indicate which variable are the ones with prominent importance. Accordingly, considering the results summarized in table 7. b_0 mainly depends on the grain size and a bit less on the Y concentration inside the tetragonal grains, whereas V_{max} mainly depends on the grain size and the amount of cubic phase.

Table 6: Summary of parameters of all samples sensitive to ageing (when necessary, b_0 and V_{max} were recalculated with $n=0.92$ and $Q=115.3$ kJ/mol)

Samples	V_{max}	b_0	Q(kJ/mol)	f: wt.% cubic	y: mol% Y_2O_3 in t	D: Grain size (nm)
1430-2h	0.82	$3.64 \cdot 10^{13}$	115.3	17.6	2.55	410
1430-5h	0.8	$3.01 \cdot 10^{13}$	115.3	20.5	2.41	520
PS1150-200h	0.85	$7.64 \cdot 10^2$	40.8	17.5	2.34	320
PS1430-20h	0.77	$4.43 \cdot 10^{13}$	115.3	30.4	2.13	750
PS1500-2h	0.79	$3.28 \cdot 10^{13}$	115.3	26.3	2.37	600
PS1550-2h	0.78	$4.75 \cdot 10^{13}$	115.3	26.8	2.34	770

Table 7. Values of the coefficients a_f , a_y , a_D in equations (7) and (8)

	a_f^b or a_f^v	a_y^b or a_y^v	a_D^b or a_D^v	$\langle b_0 \rangle$ or $\langle V_{max} \rangle$	σ_{b_0} or $\sigma_{V_{max}}$
$\frac{b_0 - \langle b_0 \rangle}{\sigma_{b_0}}$	0.12	0.57	1.05	$3.18 \cdot 10^{13}$	$1.70 \cdot 10^{13}$
$\frac{V_{max} - \langle V_{max} \rangle}{\sigma_{V_{max}}}$	-0.52	-0.26	-0.63	80.17	2.93

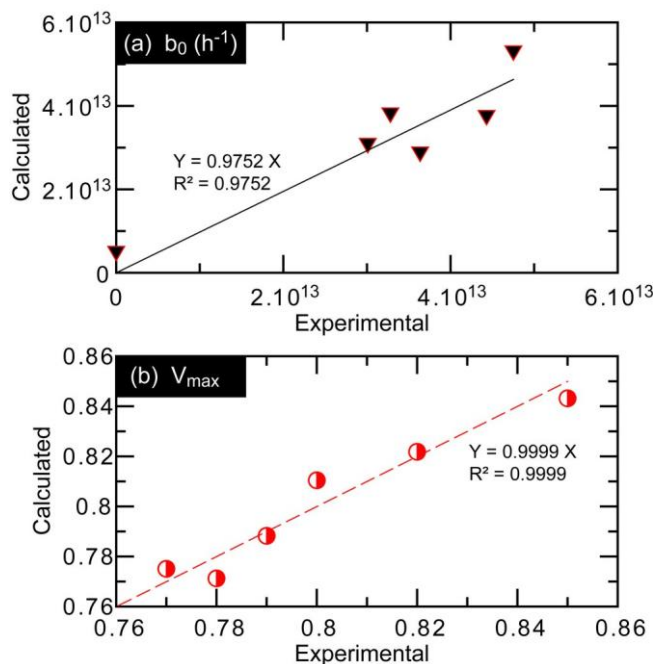


Figure 10: Comparison between experimental values of b_0 , V_{max} and values of b_0 and V_{max} recalculated from the multiple regression analysis.

4.3 Predictive ability of the phenomenological models

The models presented here (equations (4) to (8)) were established on a limited set of 9 materials obtained from a single powder. The question of their predictive power can thus be raised. To answer this, it can be interesting to compare their predictions to the microstructure and ageing kinetics of materials published by other authors [34-37].

An overall good agreement is found between the microstructural parameters measured by the different authors and the ones calculated by eq. (4) to (8) (see table 8 and figure 11 (a)). This is particularly true for grain size. However, discrepancies arise above 1600°C for Gremillard's materials: these materials (fabricated with a different powder: TZ3Y-S) exhibit a lower grain size than what is predicted by eq. (6). This could be attributed to the presence of a very small amount of amorphous phase at high temperature in TZ3YE, that can accelerate diffusion and grain growth as compared to amorphous-phase-free zirconia (such as TZ3YS). Between 1300 and 1600°C, both powders behave similarly and excellent predictions can be reached by eq. (6).

Table 8: Summary of 3YTZP ceramics studied by other authors and comparison with values calculated using eq. 4 to 8. Experimental grain sizes, wt.% cubic and mol% Y_2O_3 in t. of materials from [34] and [35] were recalculated with the methods exposed in the present article, using the micrographs shown in [34] and [35] and the original XRD data kindly provided by Dr. Inokoshi and Dr. Zhang. These data are thus different from the published ones.

	Sintering conditions		Data from other researchers			Calculated from eq. 4 to 8		
	T	t	Grain size (nm)	wt.% cubic	mol% Y_2O_3 in t	Grain size (nm)	wt.% cubic	mol% Y_2O_3 in t
Inokoshi's results[33] (In-Ceram YZ)	1450	1	388	6	3	362	16.2	2.71
	1450	2	448	23.4	2.76	438	19.0	2.55
	1450	4	537	27.6	2.57	540	22.4	2.38
	1550	1	642	24.1	2.72	599	22.1	2.46
	1550	2	806	29.7	2.52	748	26.1	2.29
	1550	4	925	32.5	2.41	938	30.4	2.17
	1650	1	1209	29.53	2.54	985	29.3	2.23
	1650	2	1537	32.4	2.41	1239	33.8	2.14
	1650	4	2522	30.1	2.39	1560	38.0	2.11
Gremillard's results (TZ3Y-S) [36]	1300	5	273			272		
	1350	5	330			335		
	1400	5	415			436		
	1450	5	500	25.1	2.41	579	23.6	2.32
	1500	5	793			768		
	1600	5	837			1310		
Zhang's Results[34] (TZ-3YE)	1650	5	1100			1680	39.3	2.09
	1350	2		4.7	2.94	278	13.7	2.80
	1400	2		9.1	2.84	341	16.0	2.68
	1450	2	438	18.4	2.60	438	19.0	2.55
	1500	2	536	30.5	2.55	573	22.3	2.41
	1550	2	722	30.5	2.49	748	26.1	2.29

Even if the correlation is less good than for grain size, the proportion of cubic phase can be reasonably well predicted for all samples. However predictions for content of Y_2O_3 in tetragonal phase are not very good for Inokoshi's materials, which may be due in particular to the fact that the total amount of yttria inside these samples (based on Vita Inceram YZ) is not precisely known (the producer of Vita InCerem YZ guarantees a weight fraction of Y_2O_3 between 4 and 6%, corresponding to a molar fraction between 2.2 and 3.6, thus this material may not be precisely a 3Y-TZP).

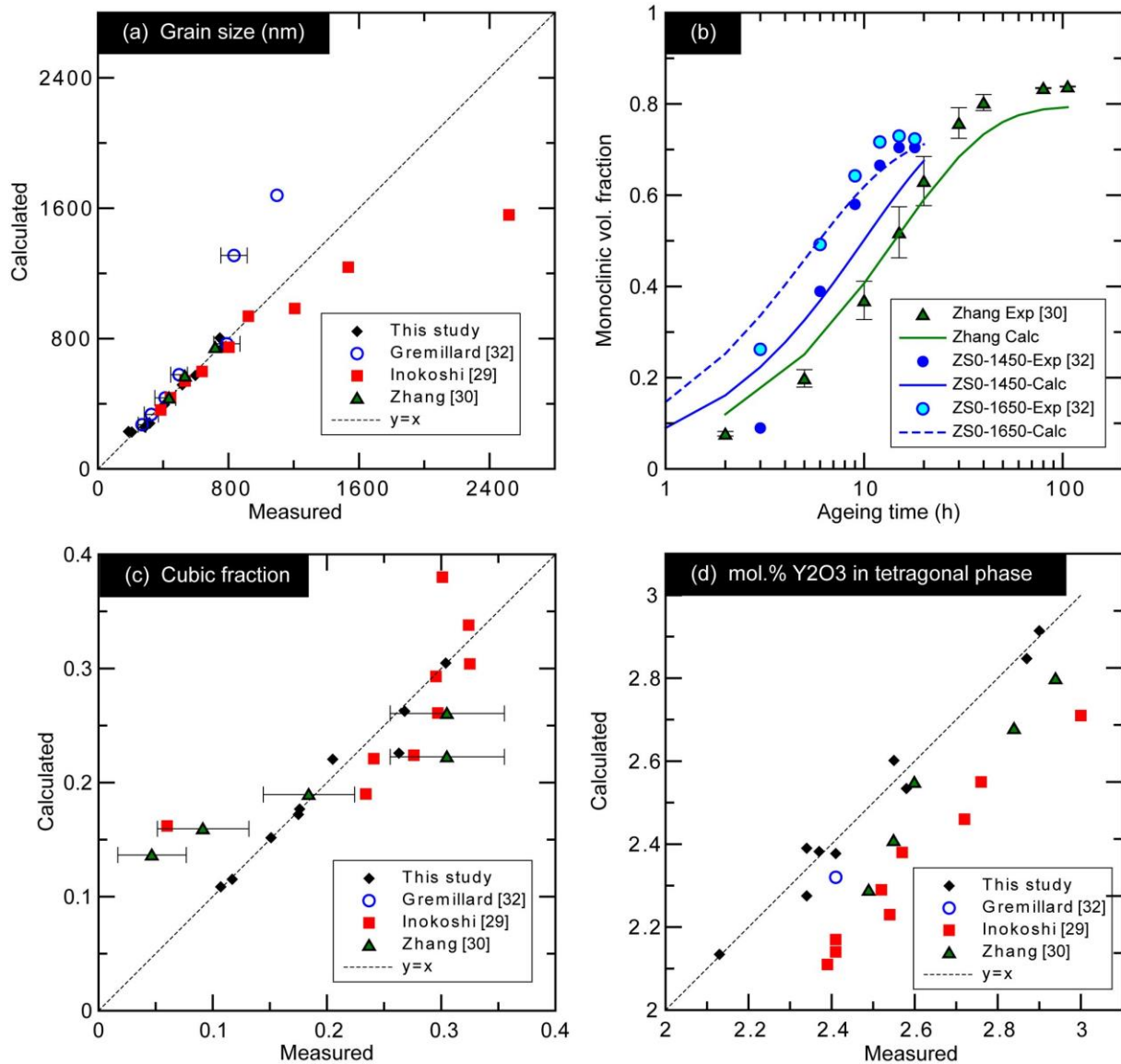


Figure 11: Comparison of the calculated and experimental values of several 3Y-TZP materials a) grain size, Inoshoki and Gremillard use other zirconia powders; b) Predicted surface phase transformation curves, compared with the experimental results of Zhang's TZ3YE sample [35] and Gremillard's TZ3YS samples [37]. Although the matches are not perfect, the orders of magnitude are correct and the ranking of samples is the same for the calculated ageing kinetics and the measured ones; c) cubic fraction; d) content of yttria in the cubic phase.

Fig.11 (b) shows ageing kinetics measured on three different materials at $134^\circ C$, together with the ones calculated with a MAJ equation using b_0 and V_{max} extrapolated from the microstructural parameters by eq. (7) and (8) (and considering $Q=115$ kJ/mol and $n=0,92$). Here we need to point out that the Q value of these samples is reported to be about 106 kJ/mol

[9], while the predicted one is 115 kJ/mol. Being unable to calculate also Q and n from the microstructural parameters is clearly a limitation of our work. Even with this limitation in mind, the correlation between measured and calculated ageing kinetics is very good for Zhang's samples. It is less good for Gremillard's samples. Indeed for these samples the experimental kinetics exhibit a n value of 3.5 and 1 respectively for ZS0-1450 and ZS0-1600, much higher than the 0.92 used here. However the orders of magnitude are correct as well as the ranking among the materials.

Although these comparisons may be biased by factors that are not considered here (internal stresses, nature of the powder...), in all cases tested here the models give rather good approximations of the real microstructure and ageing behavior of 3Y-TZP materials.

4.4 Influence of the microstructure on ageing kinetics of zirconia

In general, decreasing grain size helps to enhance zirconia ageing resistance. Here this rule applies only at 134 °C, but is not systematically valid anymore at body temperature (see the example of PS1150-200 material). This is explained by a balance between b_0 and Q . Many articles only focus on the study of Q [9] but ignore the changes in b_0 , even though both reducing b_0 and increasing Q can delay the ageing process at a given ageing temperature [4]. Here we show that each sample presents a unique combination of b_0 and Q . TSS1 and TSS2 samples do not suffer from ageing (thus b_0 and Q cannot be determined), PS1150-200h sample has the smallest b_0 and Q among all samples, and samples 1430-2h, 1430-5h, PS1430-20h, PS1500-2h, PS1550-2h have Q around 115 ± 2 kJ/mol. The differences between the last 5 samples seem to be related mostly to the grain size ($a_D^b \sim 1.1$ is the highest coefficient in eq. 7) and (a little bit less) to the content of yttrium in the tetragonal phase ($a_y^b \sim 0.57$ is the second highest coefficient in eq.7), that directly influence its stability. Indeed, lower Y content in the tetragonal grains directly means less stable tetragonal phase. The effect of grain size is less easy to explain. At least two explanations are possible. The first one is that larger grain size leads to larger internal stresses and easier transformation. The second calls on the defect structure of grain boundaries. Indeed, considering Paul's experimental results [19], when the grain size becomes smaller, the specific surface area of grain boundaries becomes higher, as well as the number of oxygen vacancies ($Y/Zr - V_O$) exposed to grain boundaries, and when their number increases to a certain extent, this leads to a dramatic change of b_0 and Q . This would also explain the difference between this group of 5 samples and PS1150-200h samples, that present the smallest grain size but similar percentage of yttrium in the t phase.

Finally, this work lacks data on Q and n . Indeed, activation energies for ageing found in the literature cover a 40 to 120 kJ/mol, however here only two groups (40 and 115) could be distinguished. As for n , in the literature values between 0.5 and 4 were found, whereas here all values of n are close to 1. Thus one can deduce that grain size, amount of yttrium in the tetragonal phase and proportion of cubic phase do not influence n . Changes in n (and Q) might then be related to other factors, such as perhaps the presence of internal and applied stresses or change in the chemistry of the zirconia powder.

5. Conclusions

In this article, we provide a predictive, phenomenological model of the influence of sintering conditions on the microstructure (amount of cubic phase, yttria content in the different phases, average grain size) of 3Y-TZP ceramics, based on results obtained on nine 3Y-TZP materials fabricated from the same powder but with different sintering cycles and validated on materials fabricated by other authors.

Moreover, we propose another phenomenological model that can approximate rather precisely the ageing behavior of 3Y-TZP materials (via the parameters n , Q , V_{\max} , V_0 and b_0 of the MAJ law describing ageing kinetics), based on their microstructure. All materials in the present study presented a n value of 0.92. From the model, it was deduced that V_{\max} has a strong linear relationship with both the content of cubic phase and the grain size. b_0 is closely linked with yttria content in the tetragonal phase and grain size.

Finally, it can be concluded that different powders can give different microstructures for a same sintering cycle. Since a strong relation was evidenced between ageing parameters and microstructural features, hydrothermal ageing of zirconia ceramics cannot always be predicted directly from processing parameters. However, it can be predicted from the microstructural features, independently of the powder used.

Acknowledgments

C. Wei was supported by a grant from the Chinese Science Council.

The authors wish to thank Dr. Fei ZHANG and Dr. Masanao INOKOSHI (K.U. Leuven) for providing the data used to establish the comparisons shown in table 8 and figure 11.

References

- [1] R.C. Garvie, R.H.J. Hannink, R.T. Pascoe, Ceramic Steel?, *Nature* 258 (1975) 703–704
- [2] J. Chevalier, What future for zirconia as a biomaterial?, *Biomaterials* 27 (2006) 535
- [3] C. Piconi, G. Maccauro, Zirconia as a ceramic biomaterial, *Biomaterials* 20 (1999) 1-25
- [4] J. Chevalier, L. Gremillard, A.V. Virkar, D.R. Clarke, The tetragonal–monoclinic transformation in zirconia: lessons learned and future trends, *J. Am. Ceram. Soc.* 92 (2009) 1901–1920
- [5] L. Gremillard, S. Meille, J. Chevalier, J. Zhao, V. Fridrici, Ph. Kapsa, J. Gereinger, J. Uribe, Degradation of bioceramics, in N. Eliaz (ed), *Degradation of Implant Materials*, Springer, New York, 2012, 195-240
- [6] X. Guo, Hydrothermal degradation mechanism of tetragonal zirconia, *J. Mater. Sci.* 36 (2001) 3737-3744
- [7] H. Schubert, F. Frey, Stability of Y-TZP during hydrothermal treatment: neutron experiments and stability considerations, *J. Eur. Ceram. Soc.* 25 (2005) 1597–1602
- [8] A. Gebressilassie, Atomic Scale Simulations in Zirconia: Effect of yttria doping and environment on stability of phases. Ph.D. Thesis, INSA-Lyon, France, 2016

- [9] J. Chevalier, B. Cales, J.M. Drouin, Low-Temperature Ageing of Y-TZP Ceramics; *J. Am. Ceram. Soc.* 82 (1999) 2150–2154
- [10] L. Gremillard, J. Chevalier, T. Epicier, S. Deville, G. Fantozzi. Modeling the ageing kinetics of zirconia ceramics; *J. Eur. Ceram. Soc.* 24 (2004) 3483
- [11] L. Gremillard, L. Martin, L. Zych, E. Crosnier, J. Chevalier, A. Charbouillot, P. Sainsot, J. Espinouse, J.-L. Aurelle, Combining ageing and wear to assess the durability of zirconia-based ceramic heads for total hip arthroplasty, *Acta Biomaterialia* 9 (2013) 7545–7555
- [12] J. Chevalier, S. Deville, E. Munch, R. Jullian, F. Lair, Critical effect of cubic phase on ageing in 3 mol% yttria-stabilized zirconia ceramics for hip replacement prosthesis, *Biomaterials* 25 (2004) 5539–45
- [13] S. Deville, J. Chevalier, L. Gremillard, Influence of surface finish and residual stresses on the ageing sensitivity of biomedical grade zirconia, *Biomaterials* 27 (2006) 2186–2192
- [14] L. Hallmann, A. Mehl, P. Ulmer, E. Reusser, J. Stadler, R. Zenobi, B. Stawarczyk, M. Özcan, C.H.F. Hämmerle, The influence of grain size on low-temperature degradation of dental zirconia, *J. Biomed. Mater. Res. Part B* 100 (2012) 447–456
- [15] S. Schmauder, U. Schubert. Significance of internal stresses for the martensitic transformation in yttria-stabilized tetragonal zirconia polycrystals during degradation. *J. Am. Ceram. Soc.* 69 (1986) 534–40
- [16] S. Deville, Etude des mécanismes de renforcement et de dégradation des céramiques biomédicales à base de zircone : du macroscopique au nanoscopique. Ph.D. Thesis, INSA-Lyon, France, 2004
- [17] J. Muñoz-Saldaña, H. Balmori-Ramirez, D. Jaramillo-Vigueras, T. Iga, G.A. Schneider. Mechanical properties and low-temperature ageing of tetragonal zirconia polycrystals processed by hot isostatic pressing. *J. Mater. Res.* 18 (2003) 2415–26
- [18] S. R. Jansen, A. J. A. Winnubst, Y. J. He, H. Verweij, P. G. Th. van der Varst and G. de With, Effects of Grain Size and Ceria Addition on Ageing Behaviour and Tribological Properties of Y-TZP Ceramics, *J. Eur. Ceram. Soc.*, 18 (1998) 557-563
- [19] A. Paul, B. Vaidhyanathan, and J.G.P. Binner, Hydrothermal Ageing Behavior of Nanocrystalline Y-TZP Ceramics, *J. Am. Ceram. Soc.*, 94 [7] (2011) 2146–2152
- [20] S. Deville, G. Guenin, J. Chevalier. Martensitic transformation in zirconia - Part I. Nanometer scale prediction and measurement of transformation induced relief. *Acta Mater.* 52 [19] (2004) 5697–5707
- [21] J. Eichler, J. Rödel, U. Eisele, M. Hoffman, Effect of grain size on mechanical properties of submicrometer 3Y-TZP: Fracture strength and hydrothermal degradation, *J. Am. Ceram. Soc.* 90 [9] (2007) 2830-2836
- [22] L. Ruiz, M. J. Readey, Effect of heat treatment on grain size, phase assemblage and mechanical properties of 3 mol% Y-TZP, *J. Am. Ceram. Soc.* 79 [9] (1996) 2331-2340
- [23] D. Bucevac, T. Kosmac, A. Kocjan, The influence of yttrium-segregation-dependent phase partitioning and residual stresses on the aging and fracture behaviour of 3Y-TZP ceramics, *Acta Biomater.* (2017), in press, <http://dx.doi.org/10.1016/j.actbio.2017.08.014>

- [24] I.-Wei Chen and X.-H. Wang, Sintering dense nanocrystalline ceramics without final-stage grain growth, *Nature* 404 (2000) 168–171
- [25] M. I. Mendelson, Average grain size in polycrystalline ceramics, *J. Am. Ceram. Soc.* 52 (1969) 443–446
- [26] H. G. Scott. Phase relationships in the zirconia-yttria system. *J. Mater. Sci.* 10 (1975)1527
- [27] F.F. Lange, D.B. Marshall, J.R. Porter. Controlling microstructures through phase partitioning from metastable precursors: the ZrO_2 – Y_2O_3 system. In J.D. MacKenzie, D.R. Ulrich (Eds.), *Ultrastructure Processing of Advanced Ceramics*, Wiley & Sons, New York (1988) 519–532
- [28] T. Stoto, M. Neuer, C. Carry, Influence of residual impurities on phase partitioning and grain growth processes of Y-TZP materials. *J. Am. Ceram. Soc.* 74 (1991) 2615–2621
- [29] H. Toraya, M. Yoshimura, S. Somiya. Calibration curve for quantitative analysis of the monoclinic tetragonal ZrO_2 system by X-rays diffraction. *J. Am. Ceram. Soc.* 67 (1984) 119–21
- [30] R.C. Garvie, P.S. Nicholson. Phase analysis in Zirconia systems. *J. Am. Ceram. Soc.* 55 (1972) 303–5
- [31] L. Gremillard, C. Wei, J. Chevalier, K. Hans, T. Oberbach. A fast, stepwise procedure to assess time-temperature equivalence for hydrothermal ageing of zirconia-based materials, *Journal of the European Ceramic Society* (2017), <http://dx.doi.org/10.1016/j.jeurceramsoc.2017.08.018>
- [32] K. Matsui, H. Horikoshi, N. Ohmichi, M. Ohgai, H. Yoshida, Y. Ikuhara, cubic-formation and grain-growth mechanisms in tetragonal zirconia polycrystal, *J. Am. Ceram. Soc.* 86 [8] (2003) 1401-8
- [33] K. Matsui, H. Yoshida, Y. Ikuhara, Isothermal Sintering Effects on Phase Separation and Grain Growth in Yttria-Stabilized Tetragonal Zirconia Polycrystal. *J. Am. Ceram. Soc.*, 92 [2] (2009) 467–475
- [34] M. Inokoshi, F. Zhang, J. De Munck, S. Minakuchi, I. Naert, J. Vleugels, B. Van Meerbeek, K. Vanmeensel. Influence of sintering conditions on low-temperature degradation of dental zirconia. *Dental materials* 30 (2014) 669–678
- [35] F. Zhang, K. Vanmeensel, M. Inokoshi, M. Batuk, J. Hadermann, B. Van Meerbeek, I. Naert, J. Vleugels. 3Y-TZP ceramics with improved hydrothermal degradation resistance and fracture toughness. *J. Eur. Ceram. Soc.*, 34 [10] (2014) 2453–2463
- [36] F. Zhang, K. Vanmeensel, M. Batuk, J. Hadermann, M. Inokoshi, B. Van Meerbeek, I. Naert, J. Vleugels. Highly-translucent, strong and ageing-resistant 3Y-TZP ceramics for dental restoration by grain boundary segregation. *Acta Biomater.*, 16 (2015) 215–222
- [37] L. Gremillard, Relations microstructure-durabilité dans une zircone biomédicale. PhD thesis, INSA-Lyon, France, 2002